EPJ Web of Conferences **343**, 02005 (2025) https://doi.org/10.1051/epjconf/202534302005
AIMACE-2025

Adaptive Biomimetic Aircraft: nature-inspired enhancement of the aerodynamic design of aircraft to improve sustainable performance

Jamila Albeshri[1], *Sura* AlOsayat[1], *Ayesha* Almehairi[1], *Yusra* Elkalyoubi[1*], and *Nafissa* El Jabban[1]

[1]Department of Physics, Dubai National School L.L.C., Dubai, United Arab Emirates

Abstract. Aviation is an essential component of the global transportation infrastructure and has experienced substantial growth in recent decades. However, this sector is also a significant contributor to global warming. The goal of this project, Adaptive Biomimetic Aircraft (ABA), is to address the problem of rising CO2 emissions in this industry by offering solutions that reduce the fuel consumption of conventional aircraft by enhancing aircraft aerodynamic design based on inspirations from nature, including shark hydrodynamics and owl flight mechanics. The first feature of ABA involves morphing wings characterized by adjustable, distinct degrees of curvature, mimicking owl wing curvature ranges, that adapt to various laminar and turbulent conditions. The second feature involves riblet microstructures, like that of shark denticles, applied to the surface of the aircraft to reduce fluid friction. Using SimScale CAE, the effects of each feature on the performance of the aircraft were studied. Five different wing models were designed and tested against varying Re values to determine the optimal design criteria for effective adaptability. Results show enhanced pressure distribution, lift-to-drag ratios, and skin friction across Re values, with marked reductions in fuel expenditure and a noteworthy decline in kilograms of CO2 emissions compared to a conventional Boeing 787-8.

1 Introduction

In 2018, civil aviation was responsible for 2.4% of the total anthropogenic fossil-fuel CO2 emissions with emissions estimated at 918 Mt CO2. [1] Driven by globalization, aviation has become a fast-growing industry, with trends of +5% growth per year. [2] By the mid-2030s, no fewer than 200,000 flights per day are expected to take off and land all over the world. [3] More recent studies suggest that aviation does not currently appear to be on track to reach a 55% reduction in emissions by 2030. [4]

According to Bergero et al., one of the most difficult emissions to minimize will be those produced from the aviation industry, due to the industry's need for energy-dense fuels that lack commercially competitive alternatives. Despite this shortage, like any other sector,

* Corresponding author: yusra.elkalyoubi@dnsalbarsha.com

aviation needs to reduce its impact on the environment and advance toward net-zero carbon emissions. [5]

This paper introduces the Adaptive Biomimetic Aircraft (ABA), an aircraft model engineered to enhance fuel efficiency and reduce CO_2 emissions. The design integrates biomimetic principles derived from two key inspirations: the flight dynamics of owls and the hydrodynamic properties of shark skin. Specifically, the model features morphing wing capabilities informed by research on owl wing adaptations to varying flight conditions and incorporates riblet surface microstructures inspired by shark skin to minimize aerodynamic drag.

Studies on avian flight provide valuable insights into efficient aerodynamic approaches. Research conducted by the Royal Veterinary College's Structure and Motion Laboratory investigated avian wing morphing under varying aerodynamic loads to inform unmanned aerial system (UAS) designs. Large birds were trained to glide through apparatuses inducing rapid and slow load changes. High-speed cameras and motion capture tracked wing shape, revealing how wing, tail, and body deform in response to turbulence. [6] While the aim of that study was to guide towards more efficient UAS designs, it has served as the foundation for the first feature of the ABA aircraft: morphing wings inspired by owl flight responses.

Riblets, inspired by the drag-reducing properties of shark skin, have garnered significant attention within the aviation industry as a potential means to enhance fuel efficiency and reduce environmental impact. Riblets function by altering turbulent boundary layer structures, minimizing skin friction drag when optimally sized and configured. Previous studies have demonstrated the potentials of these structures to reduce drag when optimally configured. [7] While existing research has focused on general riblet applications, this project explores the specific contribution of riblets on different regions of the aircraft to the overall fuel savings.

The outline of this paper is as follows: Section 2 details the design and testing methodologies for the ABA aircraft. In Section 3, the results are presented along with their analysis. The final section summarizes the study's conclusions and outlines future research directions.

2 Methods

2.1 Morphing wings

2.1.1 Determining optimal wing airfoil and morphing segments

The first feature of the ABA aircraft involves the design and testing of morphing wings. The morphing wing, inspired by the owl wing, must have an adjustable curvature range between 0 to 30 degrees, measured between leading edge to trailing edge.

To ensure an optimal design, five different morphing wings have been developed as 3D models using the SketchUp Pro [8] design tool. Each wing varied in terms of airfoil type and morphing segments. The table below breaks down the key characteristics of each wing model.

Table 1. Breakdown of wing model characteristics.

Model	Airfoil	Morphing Segment

1	Symmetrical	Trailing edge only
2	Asymmetrical	Trailing edge only
3	Round asymmetrical	Midpoint to trailing edge
4	Asymmetrical	Leading edge to trailing edge
5	Asymmetrical	Midpoint only

Testing of the models was conducted using SimScale CAE [9] software, simulating both laminar and turbulent airflow conditions in a compressible fluid flow. The performance of each wing was evaluated on the basis of the resulting pressure distribution, lift-to-drag ratio, and fluid flow across Reynolds numbers. To enact this, each wing was simulated in four distinct scenarios. The parameter settings corresponding to the "Low," "Moderate," "High," and "Standard" scenarios are detailed in Table 2.

Table 2. Parameter settings for testing scenarios for Test 1.

Parameter	**Low**	**Moderate**	**High**	**Standard**
Reynolds Number	30073770	34701987	44479371	53779150
Altitude (m)	10,000	8,000	4,000	15,000
Air Density (kg/m^3)	0.41	0.53	0.82	0.19
Dynamic Viscosity (Ns/m^2)	1.46e-5	1.53e-5	1.66e-5	1.31e-5
Air Velocity, U_y (m/s)	(0–600 iterations): 0.77 – 7.70	(0–600 iterations): 1.55 – 15.50	(0–600 iterations): 2.30 – 23	(0–600 iterations): 0.61 – 6.07
Air Velocity, U_x (m/s)	(0–600 iterations): 0	(0–600 iterations): 0	(0–600 iterations): 0	(0–600 iterations): 0
Air Velocity, U_z (m/s)	(0–600 iterations): -11.50 – -115	(0–600 iterations): -13.50 – -135	(0–600 iterations): -15.50 – -155	(0–600 iterations): -11 – -110
Air Pressure (Pa)	10325	10325	10325	10325

An optimization target was defined by comparing the average pressure ratio between the upper and lower surfaces of the conventional Boeing 787-8 wing under specific, simulated standard flight conditions. This average pressure ratio served as a baseline for evaluating the performance of the five morphing wing models. This approach was employed as an initial step to each wing model's capacity to maintain comparable aerodynamic performance to the conventional wing. It is acknowledged that pressure ratio alone is not a comprehensive indicator of aerodynamic efficiency, and further analysis considering pressure distribution, skin friction, and other drag components is necessary to fully assess the drag reduction potential of each morphing wing, especially under varying turbulence conditions.

2.1.2 Evaluating ABA wing performance against a conventional model

The best performing wing was then further enhanced with the addition leading edge extensions, including the LERX, cuff, dogtooth, and slats. A second round of testing was then conducted. In this round, the ABA aircraft was tested alongside a conventional Boeing 787-8 to provide results comparative to an existing model. Table 3 and Table 4 detail the parameter settings employed for the testing conditions for each flight phase.

Six testing scenarios, including average Angles of Attack (AoA), were defined as follows:

- Take-off: Average AoA of 15°
- Cruise (Negligible Turbulence): Average AoA of 3°
- Low Cruise: Average AoA of 4°
- Moderate Cruise: Average AoA of 5°
- High Cruise: Average AoA of 6°
- Landing: Average AoA of 3.5°

Table 3. Parameter settings for Cruise conditions for Test 2.

Parameter	**Cruise**	**Low Cruise**	**Moderate Cruise**	**High Cruise**
Reynolds Number	53779150	30073770	34701987	44479371
Air Density (kg/m^3)	0.19	0.42	0.53	0.82
Dynamic Viscosity (Ns/m^2)	1.13e-5	1.46e-5	1.53e-5	1.66e-5
Air Velocity, U_y (m/s)	(0–600 iterations): 0.61 – 6.07	(0–600 iterations): 0.87 – 8.73	(0–600 iterations): 1.18 – 11.84	(0–600 iterations): 1.63 – 16.38
Air Velocity, U_x (m/s)	(0–600 iterations): 0	(0–600 iterations): 0	(0–600 iterations): 0	(0–600 iterations): 0
Air Velocity, U_z (m/s)	(0–600 iterations): -11.58 – -115.84	(0–600 iterations): -12.49 – -124.90	(0–600 iterations): -13.52 – -135.20	(0–600 iterations): -15.58 – -155.80
Global Air Pressure (Pa)	10325	10325	10325	10325

Table 4. Parameter settings for Take-off and Landing conditions for Test 2.

Parameter	**Take-off**	**Landing**
Reynolds Number	63589371	54671500
Air Density (kg/m^3)	1.23	1.23
Dynamic Viscosity (Ns/m^2)	1.83e-5	1.83e-5
Air Velocity, U_y (m/s)	(0–600 iterations): 2.34 – 23.38	(0–600 iterations): 0.47 – 4.65
Air Velocity, U_x (m/s)	(0–600 iterations): 0	(0–600 iterations): 0
Air Velocity, U_z (m/s)	(0–600 iterations): -8.70 – -86.97	(0–600 iterations): -8.00 – -80
Global Air Pressure (Pa)	10325	10325

2.1.3 Parameter selection

The angles of attack (AoA) employed in the simulations were calculated by applying the velocity equation to the velocity components of the relative airflow. This involves resolving the airflow's velocity components and applying equation 1.

$$\alpha = \tan^{-1}\left(\frac{\boldsymbol{U_z}}{\boldsymbol{U_y}}\right) \tag{1}$$

This method assures that the AoA values are consistent with the realistic aerodynamic conditions experienced throughout various flight phases. Using this approach, the AoA values for takeoff (15°), cruise (3°-6°), and landing (3.5°) follow operational norms to the performance characteristics of commercial aircraft, which normally cruise at an AoA of around 4°-5°.

Furthermore, this methodology utilizes data collected from the International Standard Atmosphere (ISA) model to compute Reynolds numbers, which were used to define the parameters for four distinct testing conditions during the cruise phase. The Reynolds numbers were calculated using equation 2.

$$Re = \frac{\rho v d}{\mu} \tag{2}$$

where ρ is air density, v is flow speed, d is characteristic length, and μ is dynamic viscosity.

These scenarios were designed to represent different turbulence levels—negligible or standard, low, moderate, and high—based on the corresponding ranges of Reynolds numbers, reflecting variations in flow behavior under distinct atmospheric conditions.

In aerospace applications under realistic conditions, air, as a compressible fluid, typically exhibits turbulent flow, with the intensity of turbulence varying by altitude. Higher altitudes correspond to lower Reynolds numbers, while lower altitudes correspond to higher Reynolds numbers. For instance, a study on a 1/18 scale model of an aircraft wing during the cruise phase reported a Reynolds number of approximately 75 million, indicating that full-scale aircraft wings operate at Reynolds numbers in the tens of millions during cruise conditions.

In this study, distinct Reynolds numbers were selected to encompass a range of aerodynamic behaviors:

- Low Reynolds number (30073770): At this level, viscous forces dominate, resulting in weak turbulence that is more susceptible to flow separation.
- Moderate Reynolds number (34701987): At this level, the flow transitions from weak turbulence to stronger turbulence, enhancing mixing and delaying separation.
- High Reynolds number (44479371): Here, inertial forces dominate, leading to fully turbulent flow. Turbulent boundary layers at this level are more resistant to separation compared to the lower Reynolds numbers.
- Standard Reynolds number (53779150): This value represents typical operating conditions, such as cruise phase, and serves as a benchmark for performance evaluation and design optimization in this study.

2.2 Riblets

The second feature of the ABA aircraft involves riblet microstructures, inspired by shark denticles. Rhino software [10] was employed to design 3D models of these microstructures. Similar to shark denticles, the riblets' height stands between 20-30 μm with a spacing of 35-105 μm.

Once the riblets are designed, the next phase of digital construction involves applying the microstructures on different segments of an aircraft model using SketchUp Pro [8]. The Boeing 787-8 model was used as the base for the ABA riblet-enhanced models.

The placement of the riblet microstructures have been strategically selected as areas of high friction due to airflow interaction. As such, the first enhanced model contained riblets attached to the underside of the wings. The second enhanced model contained riblets attached to the underside of the fuselage.

To test the models, LES simulations were conducted using SimScale CAE [9] in the compressible flow setting.

3 Results and analysis

3.1 Morphing wings

3.1.1 Determining optimal wing airfoil and morphing segments

Fig. 1 demonstrates the pressure ratios (top to bottom) for each wing when simulated in four distinct conditions. Results from this test indicate that wing 3, with an asymmetrical airfoil and a morphing origin extending to the trailing edge, outperformed the other wing models. As depicted in the figure, wing 3 presents the most optimal and consistent results. The asymmetrical airfoil enhanced lift generation by creating a steeper pressure gradient on the wing's upper surface and a smoother gradient on the lower surface.

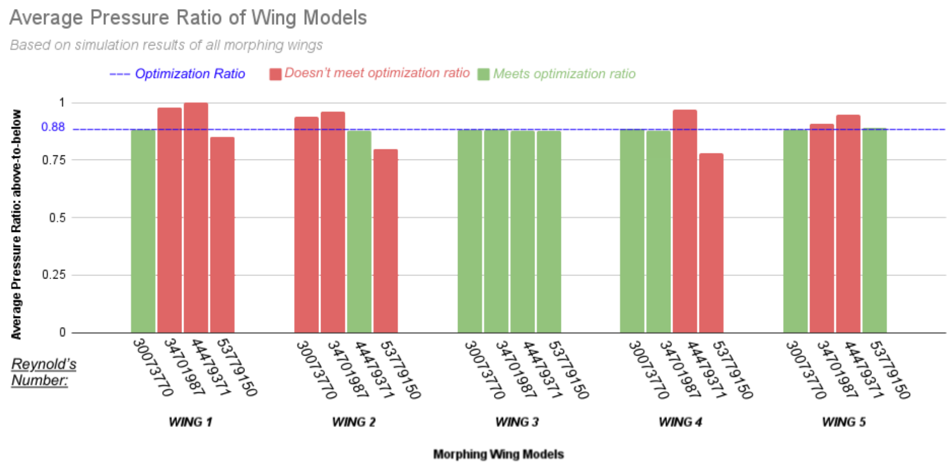

Fig. 1. Pressure ratios for each wing across various Reynolds numbers.

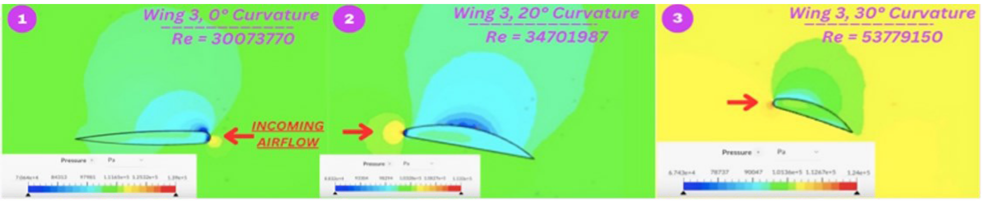

Fig. 2. Pressure distribution across wing 3 in different testing conditions.

Fig. 2 illustrates the aerodynamic performance of wing 3 under different conditions. Each panel depicts pressure distribution, demonstrating airflow patterns and regions of lift and drag, across different scenarios having varying Reynolds numbers.

3.1.2 Evaluating ABA wing performance against a conventional model

As explained earlier, the ABA wing—specifically, wing 3—is characterized by a round asymmetrical airfoil. The morphing segment begins at the midpoint until the trailing edge. The ABA wing is designed to morph from zero to 30 degrees of curvature. **Fig. 3** shows the 3D model and morphing ranges of the ABA wing.

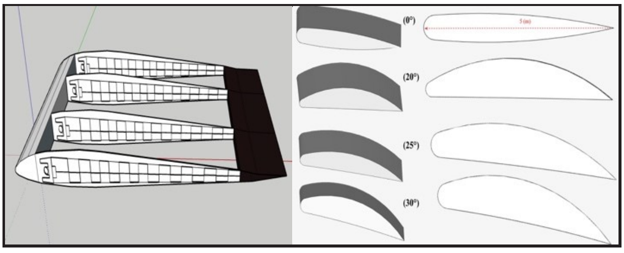

Fig. 3. 3D model of ABA wing (left), morphing range (right)

Pressure ratio results from the second test, which involved enhancements to the ABA wing and a comparison in its performance with respect to the Boeing 787-8 wing, are presented in **Fig. 4**. Furthermore, the lift-to-drag ratios for the ABA wing and the conventional Boeing 787-8 wing are presented in **Fig. 5**.

The data shows that the incorporation of leading-edge extensions, combined with morphing curvatures, increases lift force and optimizes pressure distribution around wings. This adaptability has shown to minimize energy losses due to turbulent flow and enhance aerodynamic stability. In contrast, the Boeing 787-8 wing's static design led to higher drag, particularly under turbulent scenarios.

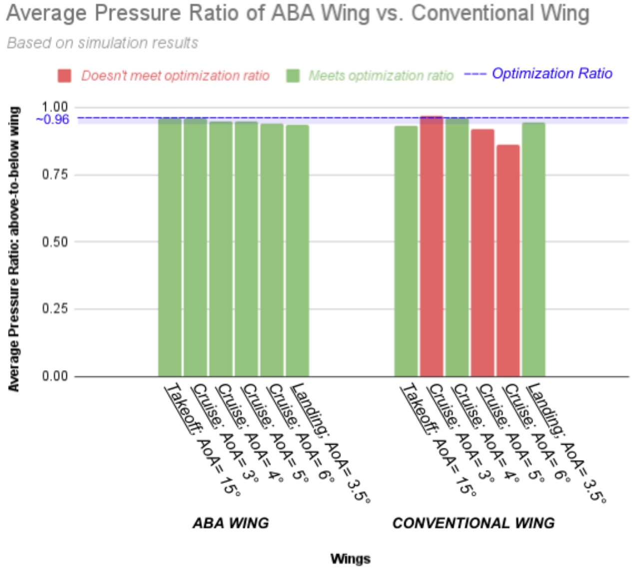

Fig. 4. Pressure ratios for ABA wing vs. Boeing 787-8 wing.

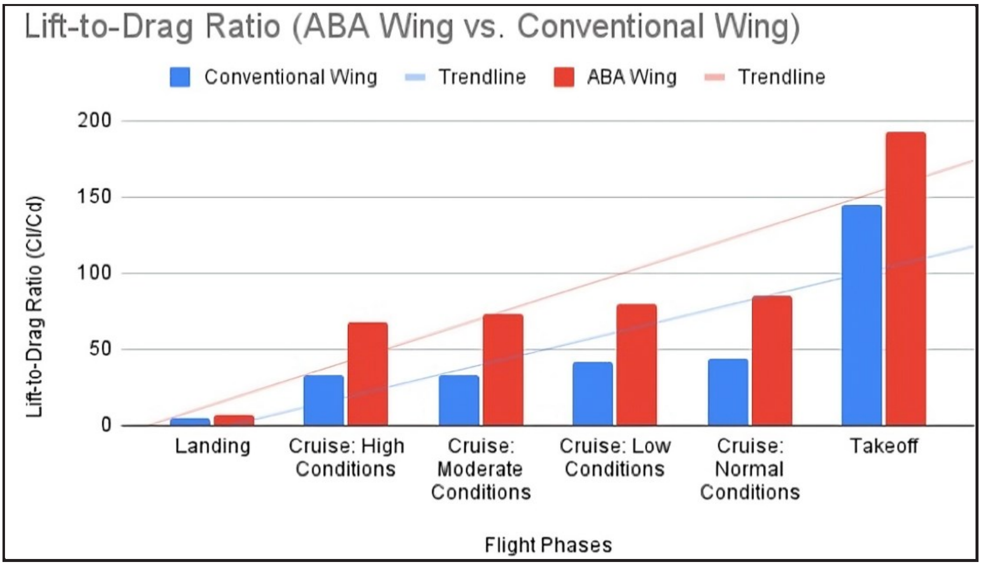

Fig. 5. Lift-to-drag ratios for ABA wing vs. Boeing 787-8 wing.

Leading edge extensions contributed to improved airflow at various angles of attack (AoA) and reduced stall during the three main phases of flight (takeoff, cruise, and landing).

Fig. 6 displays the simulation results for the ABA wing, demonstrating improved pressure distribution across flight phases. For take-off, a 15° angle of attack is optimized with a ~25° wing curvature for maximum lift. For landing, a 3.5° angle of attack matches well with a ~20° wing curvature to stabilize lift and enhance drag for safety. During cruising, wing curvature angles of ~0°, ~20°, ~25°, and ~30° efficiently stabilize lift with corresponding angles of attack of 3°, 4°, 5°, and 6°, respectively.

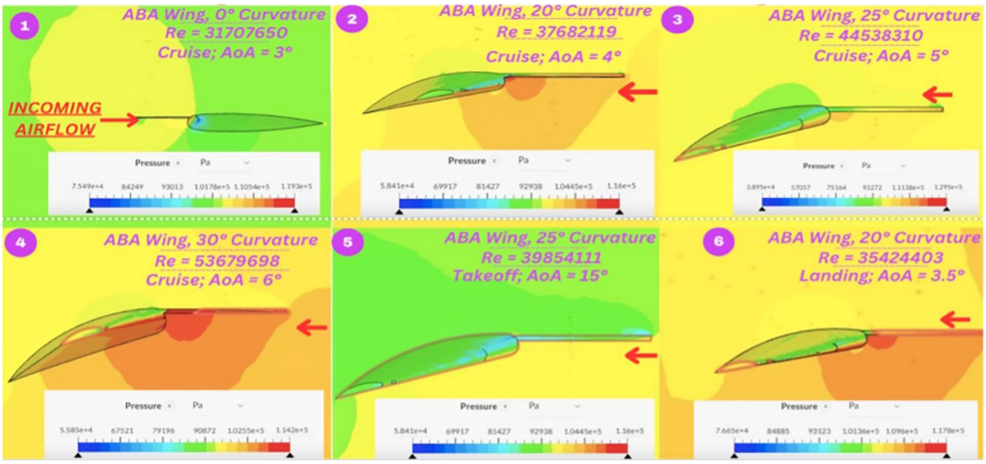

Fig. 6. Pressure distribution across the enhanced ABA wing in different testing conditions across flight phases.

3.1.3 Fuel consumption and emissions

The Boeing 787-8 typically consumes fuel at a rate of 1.84 L/s [11] and emits 3.16 kg of CO2 per kg of fuel consumed [12]. In contrast, with the implementation of the morphing wings, the ABA aircraft consumes approximately 1.20 L/s, constituting a 33% reduction in the rate of fuel consumption and a corresponding reduction in carbon emissions, assuming equivalent flight durations, as the total CO2 emitted is directly proportional to the total fuel consumed.

3.2 Riblets

Fig. 7 shows the 3D model of the riblet microstructures, digitally created using Rhino [10]. **Fig. 8** shows a magnified view of the arrangement of these microstructures when applied to the wings or the fuselage of the aircraft.

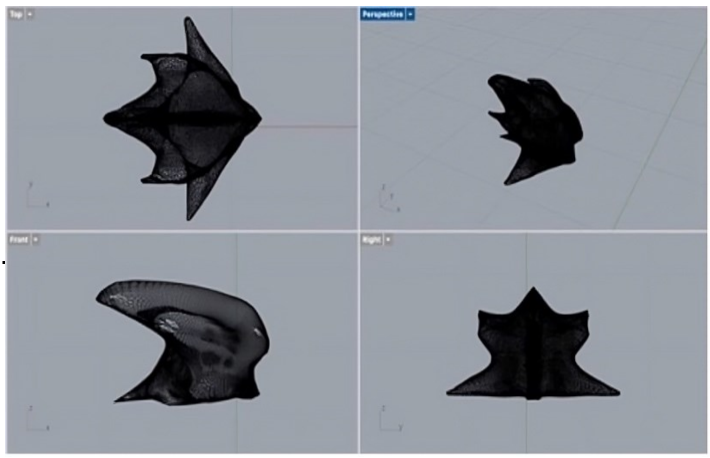

Fig. 7. All-around perspective image of the 3D modelled riblet microstructure.

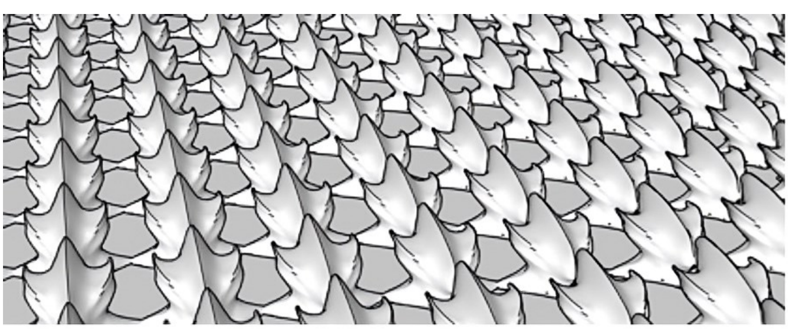

Fig. 8. Magnified view of the riblet microstructure arrangement when applied to a surface.

The riblets are shown to interact with the boundary layer, generating small, streamwise vortices that reduce skin friction drag, as depicted in **Fig. 9**.

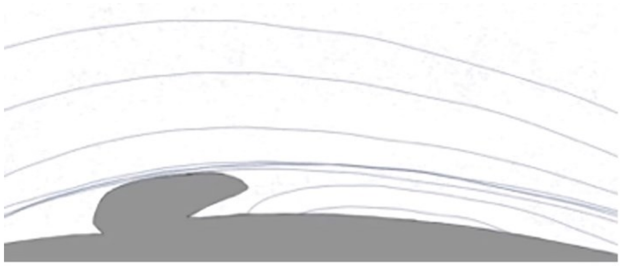

Fig. 9. Flow region around the riblet microstructure.

The conventional Boeing 787-8 aircraft model was used to display conventional performance outcomes and set a basis for comparison. **Fig. 10** displays the flow stream around the conventional aircraft.

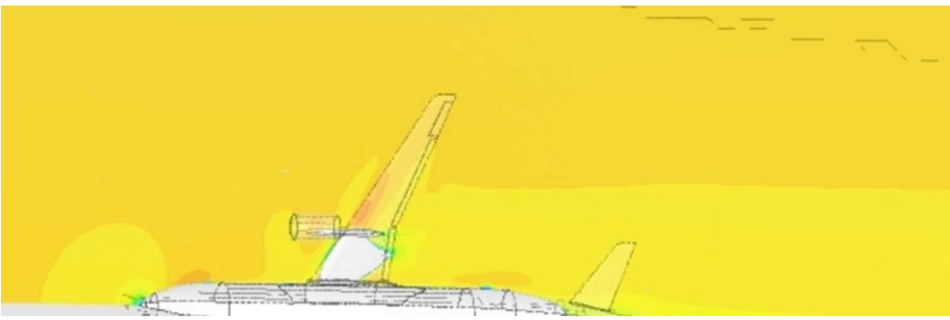

Fig. 10. Flow stream around conventional Boeing 787-8 aircraft generated using SimScale.

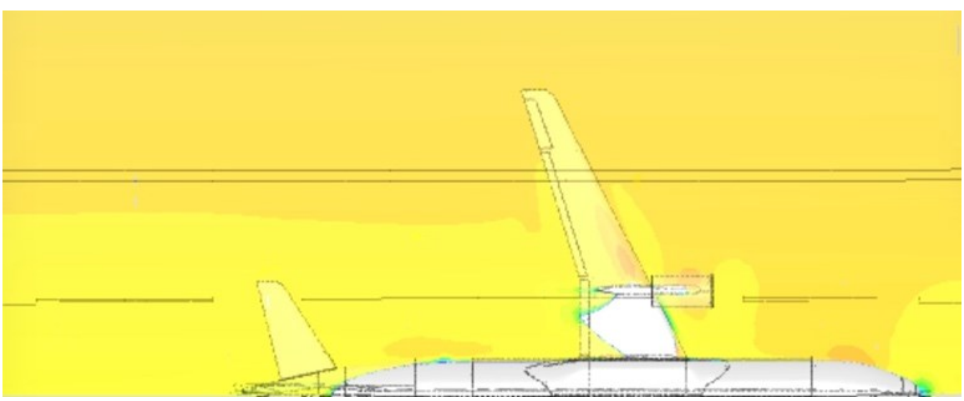

Fig. 11. Flow stream around the ABA aircraft with riblet-enhanced wings, generated using SimScale.

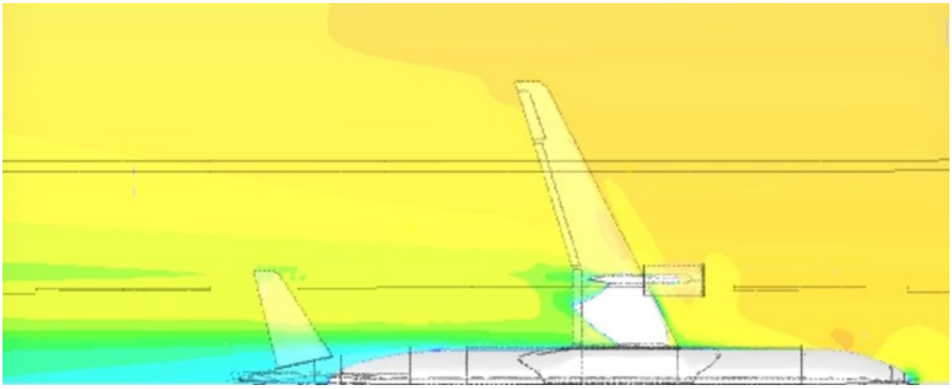

Fig. 12. Flow stream around the ABA aircraft with riblet-enhanced fuselage, generated using SimScale.

Fig. 10 demonstrates the flow stream around a convetional Boeing 787-8. Comparatively, **Fig. 11** displays the flow stream around the aircraft with riblet-enhanced wings. As shown, this particular riblet placement did not contribute to substantial changes in the airflow behind the wing. These changes, while potentially reducing drag at lower speeds, could increase drag and flow separation at higher speeds. This affected overall performance, creating a trade-off between drag reduction at lower speeds and worse performance near stall.

In contrast, results for the fuselage riblet-enhanced model, depicted in **Fig. 12**, show a 3.67% increase in flying speed. This improvement is primarily attributed to the riblets' reduction of skin friction drag within the turbulent boundary layer. By reducing the near-wall shear stress, the riblets lower the overall drag force, allowing the aircraft to achieve a higher speed for a fixed thrust setting.

With skin friction constituting approximately 50% of total drag [13], a 3.67% increase in flying speed corresponds to an estimated decrease in skin friction of 14-16%. This leads to an estimated reduction in total drag of 7.47% due to the riblets placed on the fuselage of the plane.

Given the established relationship that a 1% reduction in drag typically yields a 0.75% reduction in fuel consumption [14], the observed drag reduction achieved by implementing riblet microstructures on the fuselage is projected to result in a 5.6% improvement in fuel efficiency.

4 Conclusion

This study presented a preliminary investigation into the application of biomimetic design principles to aircraft, focusing on morphing wings inspired by owl flight and riblet microstructures inspired by shark skin. Computational fluid dynamics simulations were conducted to assess the aerodynamic performance of the proposed ABA aircraft in comparison to a conventional Boeing 787-8 aircraft baseline. Simulation results demonstrate promising reductions in drag corresponding to significant reductions in fuel consumption and CO2 emissions. However, the simulations were conducted under specific, idealized conditions, and further analysis is needed to assess performance under more realistic flight conditions, including varying turbulence levels and crosswinds. Furthermore, the relationship between skin friction reduction and fuel consumption was estimated using established approximations, warranting a more detailed analysis.

The design of an efficient aircraft is a highly iterative process. Future work will address these limitations through the development and experimental testing of a physical prototype in a wind tunnel. These tests will allow for direct measurement of aerodynamic forces and provide valuable data for validating the simulation results and further optimizing the ABA aircraft design. This iterative process will be crucial for realizing the full potential of bio-inspired design for sustainable aviation.

References

1 B. Graver, K. Zhang, D. Rutherford, CO_2 emissions from commercial aviation, 2018, International Council on Clean Transportation, (2019). Available: https://theicct.org/wp-content/uploads/2021/06/ICCT_CO2-commercl-aviation-2018_20190918.pdf/
2 M. Masiol, R. M. Harrison, Aircraft engine exhaust emissions and other airport-related contributions to ambient air pollution: A review, *Atmos. Environ., 95*, 409–455 (2014). https://doi.org/10.1016/j.atmosenv.2014.05.070
3 International Civil Aviation Organization, Future of aviation, ICAO, (n.d.). Available: https://www.icao.int/Meetings/FutureOfAviation/Pages/default.aspx
4 G. Dannet, O. Boucher, N. Bellouin, Features and evolution of civil aviation CO_2 emissions based on ADS-B data for the period between 2019–2024, *MetaSci. Aerosp., 1*, 346–370 (2024). https://doi.org/10.3934/mina.2024016
5 C. Bergero, G. Gosnell, D. Gielen, S. Kang, M. Bazilian, S. J. Davis, Pathways to net-zero emissions from aviation, *Nat. Sustain., 6*, 404–414 (2023). https://doi.org/10.1038/s41893-022-01046-9
6 R. Bomphrey, J. R. Usherwood, Avian-Inspired Multifunctional Morphing Air Vehicles: Underpinning Biological Research, Air Force Research Laboratory, European Office of Aerospace Research and Development, London, (2022).
7 M. B. Bechert, D. Bartenwerfer, G. Hoppe, W. D. Hage, A review of riblets for aerodynamic drag reduction in aviation, *Appl. Sci., 13*, 10893 (2023). https://doi.org/10.3390/app131810893
8 SketchUp, SketchUp Pro, Trimble Inc., (2024). Available: https://www.sketchup.com/en/plans-and-pricing/sketchup-pro?srsltid=AfmBOooUeItzyuao5Kgt-CeSbERpdtisfceh4R5dcLPtvRuEnkRVsass
9 SimScale, CFD, FEA, and Thermal Simulation Platform, SimScale GmbH, (2017). Available: https://www.simscale.com/
10 Rhino, Rhino 6, Robert McNeel & Associates, (2019). Available: https://www.rhino3d.com/
11 Saurabh, Fuel Consumption of Popular Aircraft, All I Know About Aviation, (2019). Available: https://alliknowaviation.com/2019/12/14/fuel-consumption-aircraft/
12 J. Overton, Fact Sheet: The Growth in Greenhouse Gas Emissions from Commercial Aviation, Environmental and Energy Study Institute (EESI), (2022). Available: https://www.eesi.org/papers/view/fact-sheet-the-growth-in-greenhouse-gas-emissions-from-commercial-aviation
13 C. Gerhold, M. Brown, C. Jasinski, Evaluation of Skin Friction Drag for Liner Applications in Aircraft, NASA, (2016). Available: https://ntrs.nasa.gov/api/citations/20160007691/downloads/20160007691.pdf
14 P. Ricco, M. Skote, M. A. Leschziner, A review of turbulent skin-friction drag reduction by near-wall transverse forcing, *Prog. Aerosp. Sci., 123*, 100713 (2021). https://doi.org/10.1016/j.paerosci.2021.100713